Geophysical Research Letters

RESEARCH LETTER
10.1029/2025GL115318

The Role of Downward Plasma Diffusion in the Ionospheric Nighttime Weddell Sea Anomaly

Quan-Han Li[1], Maosheng He[1], Wenbin Wang[2], Shun-Rong Zhang[3], Liying Qian[2], Ercha Aa[3], and Dedong Wang[4]

[1]Key Laboratory of Solar Activity and Space Weather, National Space Science Center, Chinese Academy of Sciences, Beijing, China, [2]High Altitude Observatory, National Center for Atmospheric Research, Boulder, CO, USA, [3]Haystack Observatory, Massachusetts Institute of Technology, Westford, MA, USA, [4]GFZ German Research Centre for Geosciences, Potsdam, Germany

Key Points:

- Ionospheric topside diffusive flux derived from observations is used to drive the Thermosphere Ionosphere Electrodynamics General Circulation Model (TIEGCM) model
- The TIEGCM simulation reveals that the downward plasma diffusion is indispensable for the nighttime Weddell Sea Anomaly
- Downward plasma diffusion contributes comparably to photoionization for the anomaly

Correspondence to:
M. He,
hmq512@gmail.com

Citation:
Li, Q.-H., He, M., Wang, W., Zhang, S.-R., Qian, L., Aa, E., & Wang, D. (2025). The role of downward plasma diffusion in the ionospheric nighttime Weddell Sea Anomaly. *Geophysical Research Letters*, *52*, e2025GL115318. https://doi.org/10.1029/2025GL115318

Received 12 FEB 2025
Accepted 29 MAY 2025

Abstract This study investigates the role of downward plasma diffusion in the ionospheric nighttime Weddell Sea Anomaly (WSA), characterized by an anomalous diurnal electron density peak in nighttime from the South Pacific to South America. Traditionally attributed to prolonged photoionization and ionospheric uplift during summer, the WSA is not reproduced by the latest Thermosphere Ionosphere Electrodynamics General Circulation Model. We introduce a data-driven flux approach to incorporate more realistic diffusive flux, significantly improving the model's ability to replicate key WSA features. Simulations show that topside plasma diffusion turns downward in the evening, peaking near midnight, contributing notably to the NmF2 enhancement. Around 22:00 local time, downward plasmaspheric diffusion becomes the dominant plasma source, rivaling or exceeding local photoionization (12.08 vs. 8.50 $cm^{-3}s^{-1}$ at 22:30). These results offer new insight into the interplay of processes driving the WSA and underscore the importance of plasma diffusion in ionospheric dynamics.

Plain Language Summary In the Weddell Sea region, the ionosphere exhibits unusual behavior during summer nights, as the electron densities are higher at nighttime than daytime. This phenomenon, known as the Weddell Sea Anomaly, has traditionally been explained by prolonged daylight and ionospheric uplift. In this study, we use a numerical model optimized with a data-driven approach to simulate this anomaly more accurately. Our results show that downward plasma diffusion from the plasmasphere is a crucial factor in the anomaly, especially in the evening, alongside the known role of prolonged daylight. This discovery not only advances our understanding of the anomaly but also improves our knowledge of how the plasmasphere and ionosphere interact, with implications for space weather forecasting and related model development.

1. Introduction

The ionospheric nighttime Weddell Sea Anomaly (WSA) is characterized by an enhanced electron density during local summer nights compared to daytime levels. This phenomenon was first identified through ionosonde observations near the Weddell Sea region, specifically at Halley Bay (75.5°S, 26.6°W; Bellchambers & Piggott, 1958) and the Argentine Islands (65.3°S, 64.3°W; Dudeney & Piggott, 1978). Subsequent studies have revealed that this summer nighttime anomaly extends over a broad region, spanning from the South Pacific to South America and Antarctic (Horvath & Essex, 2003). A similar day-night anomaly has also been observed in the Northern Hemisphere, notably over East Asia and the North Atlantic (Chang et al., 2015; Feng et al., 2023; He et al., 2009; Hsu et al., 2011; Lin et al., 2009, 2010; Slominska et al., 2020; Yin et al., 2022). These summer anomalies predominantly occur at longitudes where the geomagnetic equator is displaced poleward relative to the geographic equator (e.g., Lin et al., 2010), and exhibit opposite dependencies on geomagnetic declination between the Northern and Southern hemispheres (He et al., 2009). As a result, these features are collectively referred to by several terms, including the general WSA (He et al., 2009), the summer evening anomaly (Burns et al., 2011), and the midlatitude summer nighttime anomaly (MSNA; Lin et al., 2010; Thampi et al., 2009). In this study, we follow the terminology of He et al. (2009) and use the term general WSA to collectively describe the classical WSA and similar nighttime electron density enhancements observed across a wider range of longitudes.

The phenomenon is primarily attributed to the combined effect of prolonged photoionization during the summer months and wind-driven uplift of the ionosphere (e.g., Y. Chen et al., 2016; He et al., 2009; Horvath, 2006; Jee et al., 2009; Liu et al., 2010). In addition, several studies have proposed that downward plasma diffusion from the

plasmasphere could contribute to the anomaly (e.g., Burns et al., 2008, 2011; Evans, 1965; Li et al., 2018, 2023). However, direct evidence supporting the diffusion mechanism remains elusive due to the challenges in measuring the diffusive flux directly.

Numerical simulations have provided further insights into the mechanism of the anomaly (Bravo et al., 2024; Cai et al., 2022; C. H. Chen et al., 2013; Ren et al., 2012; Richards et al., 2017; Thampi et al., 2011). For instance, C. H. Chen et al. (2011) used the SAMI2 (Sami2 is Another Model of the Ionosphere) to simulate the WSA, identifying equatorward neutral wind as the primary driver and downward plasma diffusion as an additional source. However, their analysis, which focused on the total plasma velocity/flux, did not differentiate between the specific contributions of diffusion, wind-driven transport, and plasma E × B drift. Despite these advances, the exact role of downward plasma diffusion in the WSA remains unresolved, hindering a complete understanding of the underlying physical mechanisms.

In this study, we aim to address this issue using a method similar to Li et al. (2024). They incorporated a global diffusive flux from observations into the upper boundary condition of the Thermosphere Ionosphere Electrodynamics General Circulation Model (TIEGCM), successfully reproducing the winter nighttime electron density enhancement. This demonstrated that including the data-driven diffusive flux has improved the model's ability to simulate the nighttime ionosphere. The latest version of TIEGCM still cannot reproduce WSA, which is a long-standing and significant challenge to the ionosphere community (e.g., Jee et al., 2009). In this study, we apply the same approach to improve the model performance on WSA, and quantitatively evaluate the role of downward plasma diffusion in the phenomenon and investigate the contributions of competing mechanisms.

2. Model Description

The TIEGCM is a three-dimensional, time-dependent, numerical model of the Earth's coupled thermosphere-ionosphere system (Richmond et al., 1992). In the model, the O^+ solver treats the plasma transport to and from the plasmasphere by specifying the diffusive flux at the upper boundary. By default, TIEGCM employs a simplified assumption for this flux, represented as a globally fixed constant: an upward flux of 2×10^8 cm^{-2}s^{-1} during the day and a downward flux of -2×10^8 cm^{-2}s^{-1} at night.

In this study, we perform two model runs to assess the effects of different boundary conditions on ionospheric simulations of the WSA. One run utilizes the default constant diffusive flux values, while the other integrates a more realistic flux derived from ionospheric observations, as described in Li et al. (2024). This method aims to provide a more accurate depiction of real topside flux conditions. This study focuses on the Southern Hemisphere part of the general WSA, therefore our simulations are configured for the 357th day of the year 2008, to reflect this seasonal and geographic context.

3. Results and Discussion

3.1. Model Performance

Figure 1 displays the global distribution of simulated NmF2. At 14:00 LT, both runs reveal similar global patterns, with a prominent equatorial ionization anomaly (EIA). At 00:00 LT, NmF2 from the default (constant) diffusive flux run also shows the EIA in the equatorial and low latitude regions but with significantly lower values. As a result, NmF2 difference between 00:00 and 14:00 LT is mostly negative, indicating that daytime NmF2 is higher than nighttime NmF2 over the Southern Hemisphere. In contrast, at 00:00 LT, NmF2 from the run using the derived (realistic) diffusive flux is notably higher at midlatitudes in the Southern Hemisphere, especially around the South Pacific and South America. This leads to the positive night-day NmF2 difference extending broadly from 120°E to 30°W longitude that is consistent with the features of WSA in the South American sector and similar but lower-latitude nighttime electron density enhancements located outside the classic WSA region, as reported in prior studies by ground TEC (e.g., Feng et al., 2023), as well as satellite in-situ (e.g., Liu et al., 2010; Slominska et al., 2014; Xiong & Lühr, 2014; Zakharenkova et al., 2017) and remote-sensing measurements (e.g., Hsu et al., 2011; Zakharenkova et al., 2017).

Figure 2 depicts the Southern Hemisphere distribution of the simulated hmF2, and the two model runs show similar results. At 14:00 LT, hmF2 is much higher in the equatorial region than at other latitudes. In comparison, at 00:00 LT, it decreases at equator and increases at midlatitude, especially around South America, which is also a

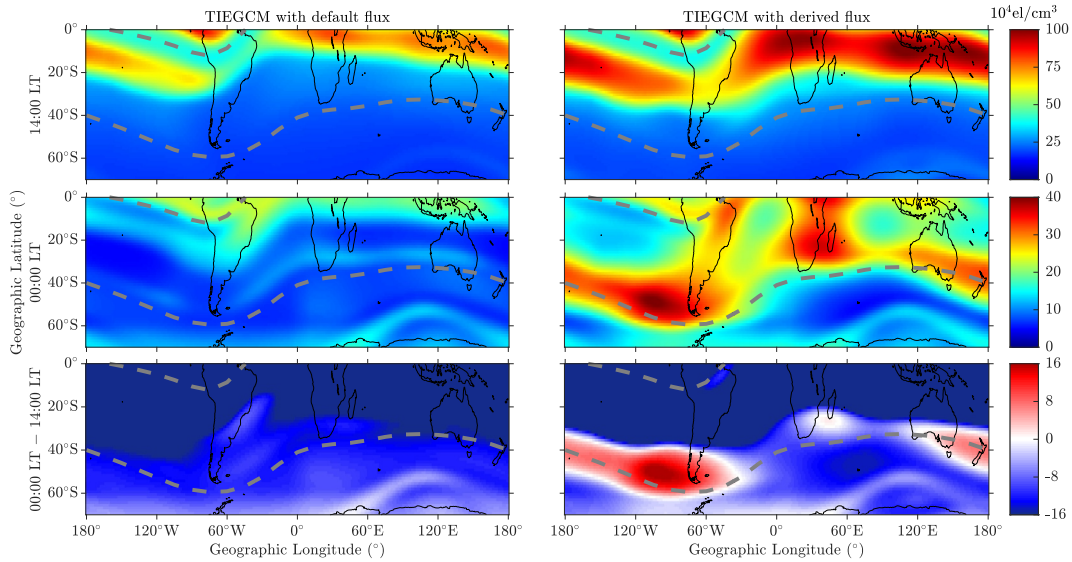

Figure 1. Global distribution of NmF2 at (top row) 14:00 LT, (middle row) 00:00 LT and (bottom row) the difference between them. The left and right columns show results from Thermosphere Ionosphere Electrodynamics General Circulation Model simulations using the default and derived diffusive flux, respectively. The dashed lines denote 0° and 45°S geomagnetic latitudes.

general WSA feature reported by previous ionosonde (e.g., Richards et al., 2017) and satellite observations (e.g., Burns et al., 2008; Y. Chen et al., 2016; He et al., 2009).

3.2. Quantitative Assessment of Diffusion and Competing Mechanisms

Using the data-driven diffusive flux significantly enhances the model's ability to reproduce the general WSA, highlighting the importance of plasma diffusion in the phenomenon. To quantitatively assess the diffusion impact, we present the distribution of the derived diffusive flux at the upper boundary of TIEGCM alongside the NmF2 change rate (dNmF2/dt) due to diffusion, calculated by the model's O^+ solver, as shown in Figure 3.

At 16:00 LT, the topside diffusive flux is predominantly upward, except in some low and high-latitude regions, leading to a negative NmF2 change rate. By 18:00 LT, the flux at midlatitudes shifts downward, intensifying from

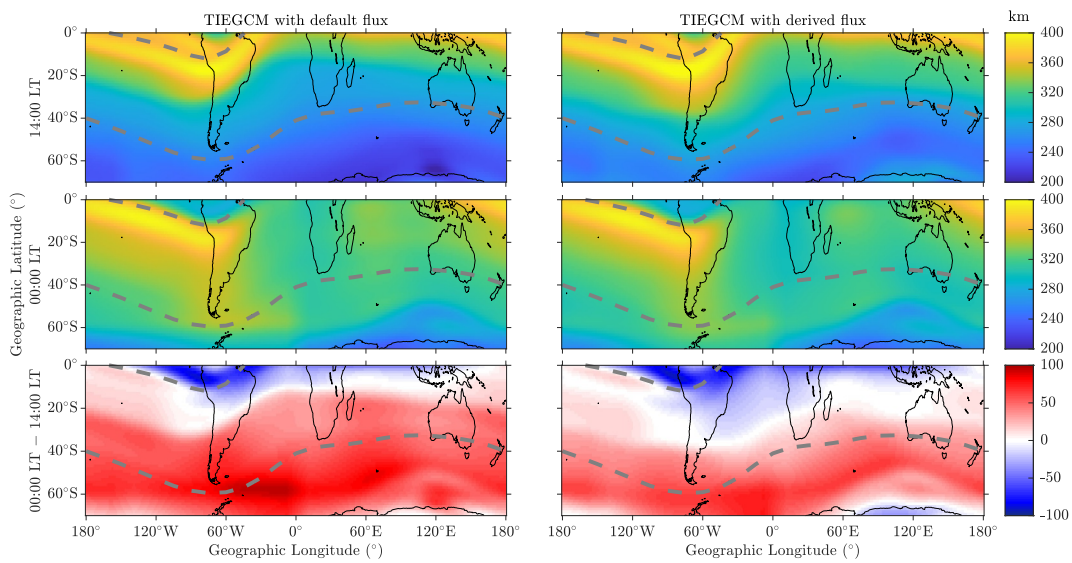

Figure 2. Similar to Figure 1 but for hmF2.

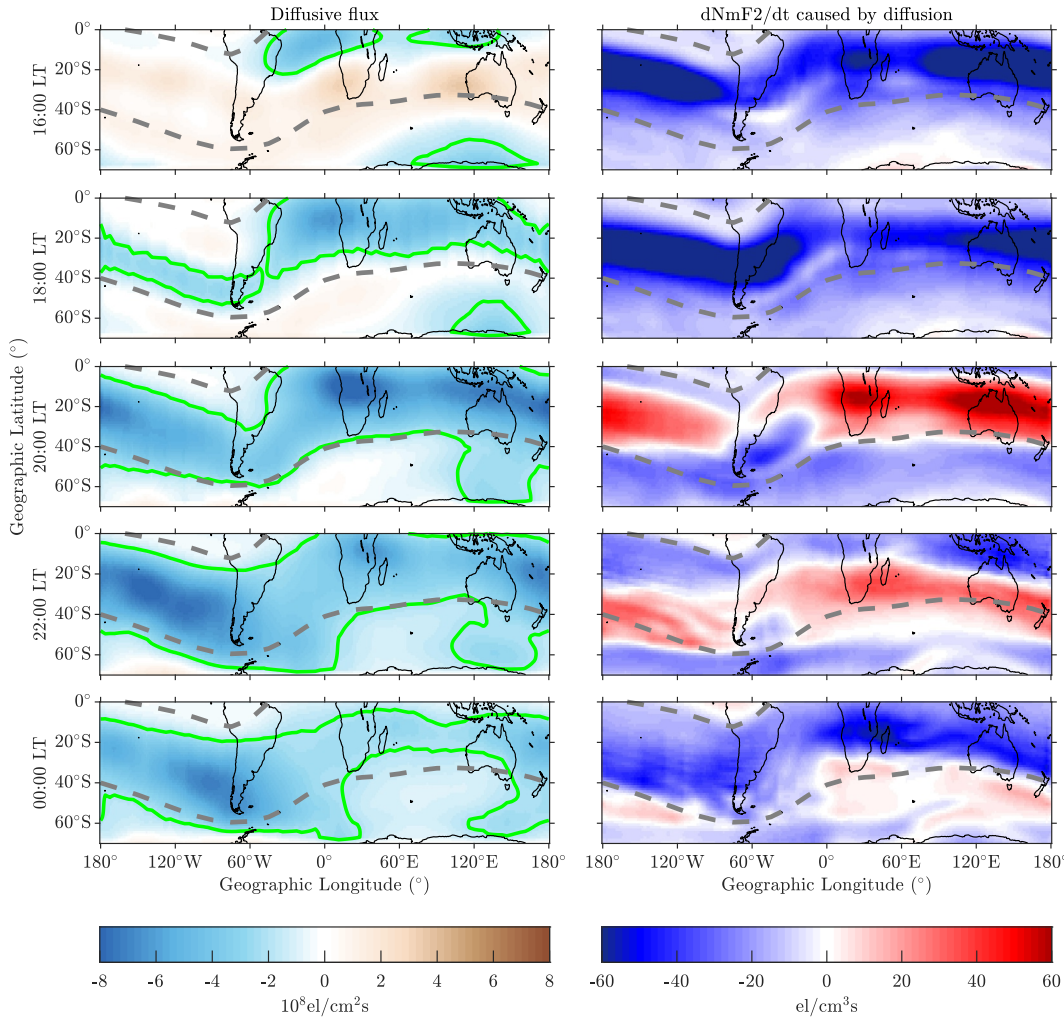

Figure 3. Distribution of (left column) the derived diffusive flux at the upper boundary of Thermosphere Ionosphere Electrodynamics General Circulation Model and (right column) the NmF2 change rate (dNmF2/dt) due to diffusion. The dashed lines denote 0° and 45°S geomagnetic latitudes, the green solid lines represent contours of -2×10^8 cm^{-2}s^{-1}.

20:00 to 22:00 LT, with higher values around the South Pacific, South Africa, and Australia. This shift results in a positive NmF2 change rate starting at 20:00 LT, with increased values in these regions. By 00:00 LT, the downward flux begins to decrease, and the positive NmF2 change rate drops significantly. Notably, the derived midlatitude flux is generally larger than the model's default fixed value of -2×10^8 cm^{-2}s^{-1}, indicated by the green solid lines. This suggests that the default model underestimates downward plasma diffusion during the Southern Hemisphere summer and its role in general WSA formation. This discrepancy likely explains the absence of general WSA in the default TIEGCM results.

Finally, to compare the effect of downward plasma diffusion with other competing mechanisms of WSA, we perform a term analysis of the O^+ solver in the model with the derived diffusive flux. This analysis examines the NmF2 change rate resulting from various chemical and transport processes, as shown in Figure 4. The left panel presents results from the general WSA peak region (55°S, 90°W). The total change rate (black line) is positive from 14:00 to 23:30 LT, except between 19:30 and 21:00 LT when it slightly dips. This indicates a general increase in NmF2. Photoionization is the primary contributor to this increase. Meanwhile around 22:00 LT downward plasma diffusion becomes another major factor, comparable to photoionization as the latter's continuous diminishing. Its effect maximizes at 22:30 LT, the resulting NmF2 change rate is 12.08 cm^{-3}s^{-1} which exceeds photoionization production rate of 8.50 cm^{-3}s^{-1}. The contribution of E × B drift is close to zero

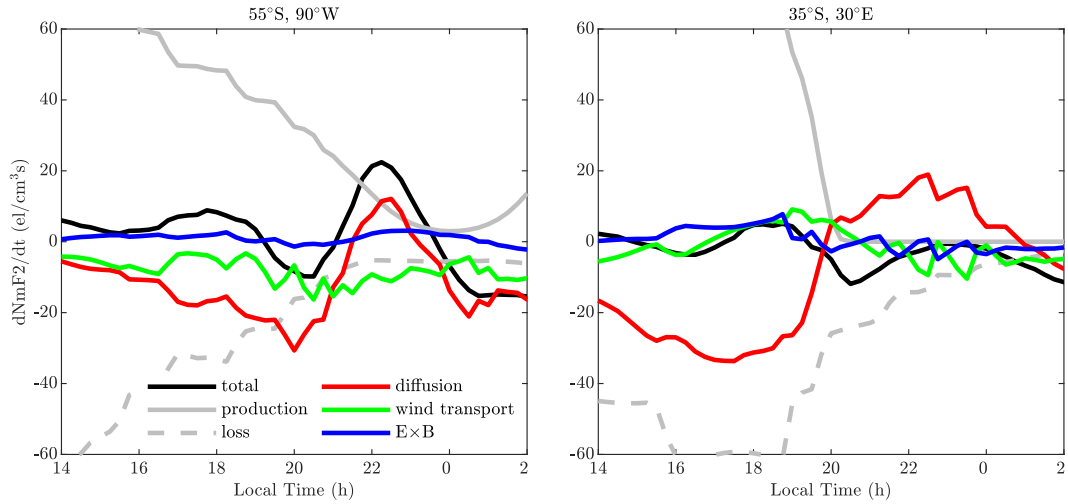

Figure 4. Local time variation of the NmF2 change rate (dNmF2/dt) from the Thermosphere Ionosphere Electrodynamics General Circulation Model simulation using the derived diffusive flux, at (left) 55°S, 90°W and (right) 35°S, 30°E. The black lines denote the total NmF2 change rate. The gray solid and dashed lines denote the NmF2 change rate caused by photoionization production and chemical loss, respectively. The red, green and blue lines denote the NmF2 change rate caused by diffusion, neutral wind transport and E × B drift, respectively.

(the resulting NmF2 change rate at 22:30 is 3.03 $cm^{-3}s^{-1}$), and that of neutral wind transport is negative. On the other hand, the chemical loss rate decreases continuously due to ionospheric uplift, as shown in Figure 2.

The question of why TIEGCM is unable to replicate a sunlit ionosphere over the WSA is of much current interest. Our analysis suggests that besides photoionization along with hmF2 uplift, downward plasma diffusion is also essential for general WSA formation. To verify this, we also present results from outside the general WSA region (35°S, 30°E) in the right panel of Figure 4. Although the NmF2 change rate from diffusion is high at night, the total change rate turns negative after 15:00 LT and only becomes slightly positive around 18:00 LT. This is not enough to surpass the NmF2 at 14:00 LT. The rapid decline of photoionization in the afternoon and its absence after 20:30 LT, coupled with the elevated chemical loss rate due to the weak ionospheric uplift in this region (Figure 2), explains this pattern.

Verifying the good performance of the customized TIEGCM model used, the simulation results correctly demonstrate that prolonged photoionization and ionospheric uplift during summer serve as essential background conditions for the formation of the WSA. Around 22:00 LT, downward plasma diffusion emerges as a key contributor, exhibiting a magnitude comparable to the enhancements driven by photoionization. Notably, our findings also point to potential interactions between these physical processes. As illustrated in Figure 2, the ionospheric uplift in the simulation using enhanced (derived) diffusive flux is relatively weaker than that in the simulation with smaller (default) diffusion. For instance, at the general WSA peak region (55°S, 90°W), the difference in hmF2 between 00:00 and 14:00 LT is 57 km in the enhanced diffusion case, compared to 78 km in the default case. Correspondingly, the chemical loss rate at 00:00 LT is more negative in the enhanced diffusion run (-5.51 $cm^{-3}s^{-1}$) than in the default run (-0.70 $cm^{-3}s^{-1}$, not shown). These comparisons suggest that a stronger downward diffusive flux can mitigate the impact of wind-driven uplift. The complex interplay between diffusion and neutral wind dynamics warrants further investigation in future studies.

This study addresses the long-standing issue of why TIEGCM fails to reproduce the WSA, emphasizing the critical role of downward plasma diffusion in its formation. In contrast to previous numerical studies (e.g., C. H. Chen et al., 2011), our work provides the first quantitative evaluation of the relative contributions of downward diffusion and other mechanisms, offering a more detailed and comprehensive understanding of the underlying physical processes responsible for this phenomenon.

4. Summary and Remarks

This study quantitatively investigates the role of downward plasma diffusion in the formation of the general WSA using TIEGCM simulations, incorporating data-derived diffusive flux as the upper boundary condition. For comparison, simulations using the default (uniformly distributed) flux are also performed. The key findings are summarized as follows:

1. The TIEGCM simulation with the default (constant) diffusive flux fails to reproduce the general WSA. In contrast, the simulation using the derived (realistic) flux successfully captures key WSA characteristics, including its spatial distribution and associated hmF2 uplift.
2. In the Southern Hemisphere midlatitude regions, the topside diffusive flux reverses to a downward direction at approximately 18:00 LT and intensifies toward 00:00 LT, with peak magnitudes occurring over the South Pacific, South Africa, and Australia. This leads to a positive NmF2 change rate between 20:00 and 22:00 LT, with a local NmF2 maximum near midnight in these regions.
3. Term analysis reveals that sustained photoionization and ionospheric uplift during summer provide essential background conditions for WSA formation. Around 22:00 LT, downward plasma diffusion becomes a critical plasma source, with a contribution comparable to, or even exceeding, that of photoionization. Specifically, at 22:30 LT, the NmF2 change rates due to diffusion and photoionization are 12.08 and 8.50 $cm^{-3}s^{-1}$, respectively.

The primary uncertainties in the derived flux arise from the use of empirical ion and electron temperatures (T_i and T_e) and neutral densities. For example, a 10% variation in $T_i + T_e$ leads to an approximate 5 m/s change in the calculated diffusive velocity at hmF2 + 100 km altitude (G. Chen et al., 2009). Although T_e is scaled using satellite observations and the derived velocity exhibits consistency in magnitude and local time variation with incoherent scatter radar measurements (Li et al., 2024), the TIEGCM upper boundary (400–500 km altitude) is close to hmF2. As a result, flux uncertainties can significantly impact simulated NmF2. Future work should aim to enhance the accuracy of the flux input through higher-precision observational data and further refinement of physical models.

Data Availability Statement

The simulation results in this study are available at Li (2025). TIEGCM is provided by the National Center for Atmospheric Research (https://www.hao.ucar.edu/modeling/tgcm/).

Acknowledgments
This work is supported by the Strategic Priority Research Program of Chinese Academy of Sciences (Grant XDA0470301), the Project of Stable Support for Youth Team in Basic Research Field, CAS (YSBR-018), and the National Key R&D program of China (2021YFE0110200).

References

Bellchambers, W. H., & Piggott, W. R. (1958). Ionospheric measurements made at Halley Bay. *Nature*, *182*(4649), 1596–1597. https://doi.org/10.1038/1821596a0

Bravo, M., Villalobos, C., Rivera, C. C., Foppiano, A., & Ovalle, E. (2024). Seasonal evolution of the ionospheric summer evening and Weddell Sea anomalies: Antarctic Peninsula area. *Advances in Space Research*, *75*(6), 4740–4755. https://doi.org/10.1016/j.asr.2024.12.047

Burns, A. G., Solomon, S. C., Wang, W., Jee, G., Lin, C. H., Rocken, C., & Kuo, Y. H. (2011). The summer evening anomaly and conjugate effects. *Journal of Geophysical Research*, *116*(A1), 7. https://doi.org/10.1029/2010ja015648

Burns, A. G., Zeng, Z., Wang, W., Lei, J., Solomon, S. C., Richmond, A. D., et al. (2008). Behavior of the F2 peak ionosphere over the South Pacific at dusk during quiet summer conditions from COSMIC data. *Journal of Geophysical Research: Space Physics*, *113*(A12), A12305. https://doi.org/10.1029/2008ja013308

Cai, Y., Yue, X., Wang, W., Zhang, S., Liu, H., Lei, J., et al. (2022). Ionospheric topside diffusive flux and the formation of summer nighttime ionospheric electron density enhancement over millstone hill. *Geophysical Research Letters*, *49*(4), e2021GL097651. https://doi.org/10.1029/2021gl097651

Chang, F. Y., Liu, J. Y., Chang, L. C., Lin, C. H., & Chen, C. H. (2015). Three-dimensional electron density along the WSA and MSNA latitudes probed by FORMOSAT-3/COSMIC. *Earth Planets and Space*, *67*(1), 156. https://doi.org/10.1186/s40623-015-0326-8

Chen, C. H., Huba, J. D., Saito, A., Lin, C. H., & Liu, J. Y. (2011). Theoretical study of the ionospheric Weddell Sea Anomaly using Sami2. *Journal of Geophysical Research*, *116*(A4), 116. https://doi.org/10.1029/2010ja015573

Chen, C. H., Lin, C. H., Chang, L. C., Huba, J. D., Lin, J. T., Saito, A., & Liu, J. Y. (2013). Thermospheric tidal effects on the ionospheric midlatitude summer nighttime anomaly using Sami3 and TIEGCM. *Journal of Geophysical Research: Space Physics*, *118*(6), 3836–3845. https://doi.org/10.1002/jgra.50340

Chen, G., Xu, J., Wang, W., Lei, J., & Deng, Y. (2009). Field-aligned plasma diffusive fluxes in the topside ionosphere from radio occultation measurements by CHAMP. *Journal of Atmospheric and Solar-Terrestrial Physics*, *71*(8–9), 967–974. https://doi.org/10.1016/j.jastp.2009.03.027

Chen, Y., Liu, L., Le, H., Wan, W., & Zhang, H. (2016). The global distribution of the dusk-to-nighttime enhancement of summer NmF2 at solar minimum. *Journal of Geophysical Research: Space Physics*, *121*(8), 7914–7922. https://doi.org/10.1002/2016ja022670

Dudeney, J. R., & Piggott, W. R. (1978). Antarctic ionospheric research. In *Upper atmosphere research in Antarctica* (pp. 200–235). American Geophysical Union (AGU). https://doi.org/10.1029/AR029p0200

Evans, J. V. (1965). Cause of the mid-latitude evening increase in to F2. *Journal of Geophysical Research*, *70*(5), 1175–1185. https://doi.org/10.1029/jz070i005p01175

Feng, J., Wang, K., Li, W., Han, B., Zhao, Z., Zhang, T., & Meng, D. (2023). Analysis of temporal and spatial variation characteristics of midlatitude summer nighttime anomaly in low and middle solar activity period. *Advances in Space Research*, *71*(10), 4351–4360. https://doi.org/10.1016/j.asr.2022.12.039

He, M., Liu, L., Wan, W., Ning, B., Zhao, B., Wen, J., et al. (2009). A study of the Weddell Sea Anomaly observed by FORMOSAT-3/COSMIC. *Journal of Geophysical Research*, *114*(A12), 12309. https://doi.org/10.1029/2009ja014175

Horvath, I. (2006). A total electron content space weather study of the nighttime Weddell Sea Anomaly of 1996/1997 southern summer with TOPEX/Poseidon radar altimetry. *Journal of Geophysical Research*, *111*(A12), 111. https://doi.org/10.1029/2006ja011679

Horvath, I., & Essex, E. (2003). The Weddell sea anomaly observed with the Topex satellite data. *Journal of Atmospheric and Solar-Terrestrial Physics*, *65*(6), 693–706. https://doi.org/10.1016/s1364-6826(03)00083-x

Hsu, M. L., Lin, C. H., Hsu, R. R., Liu, J. Y., Paxton, L. J., Su, H. T., et al. (2011). The O I 135.6 nm airglow observations of the midlatitude summer nighttime anomaly by TIMED/GUVI. *Journal of Geophysical Research: Space Physics*, *116*(A7), A07313. https://doi.org/10.1029/2010ja016150

Jee, G., Burns, A. G., Kim, Y., & Wang, W. (2009). Seasonal and solar activity variations of the Weddell Sea Anomaly observed in the TOPEX total electron content measurements. *Journal of Geophysical Research*, *114*(A4), A04307. https://doi.org/10.1029/2008ja013801

Li, Q. (2025). The role of downward plasma diffusion in the ionospheric Weddell Sea Anomaly [Dataset]. https://doi.org/10.17605/OSF.IO/F3982

Li, Q., Hao, Y., Guo, J., Zhang, X., Zhang, D., Xiao, Z., & Cui, J. (2023). Winter nighttime enhancement of the midlatitude ionosphere: Contribution from the diffusive and wind-driven plasma transport. *Journal of Geophysical Research: Space Physics*, *128*(3), 325. https://doi.org/10.1029/2022ja031108

Li, Q., Hao, Y., Wang, W., Zhang, S., Qian, L., Aa, E., et al. (2024). Global distribution of ionospheric topside diffusive flux and midlatitude electron density enhancement in winter nighttime. *Geophysical Research Letters*, *51*(24), e2024GL111091. https://doi.org/10.1029/2024gl111091

Li, Q., Hao, Y., Zhang, D., & Xiao, Z. (2018). Nighttime enhancements in the midlatitude ionosphere and their relation to the plasmasphere. *Journal of Geophysical Research: Space Physics*, *123*(9), 7686–7696. https://doi.org/10.1029/2018ja025422

Lin, C. H., Liu, C. H., Liu, J. Y., Chen, C. H., Burns, A. G., & Wang, W. (2010). Midlatitude summer nighttime anomaly of the ionospheric electron density observed by FORMOSAT-3/COSMIC. *Journal of Geophysical Research*, *115*(A3), A03308. https://doi.org/10.1029/2009ja014084

Lin, C. H., Liu, J. Y., Cheng, C. Z., Chen, C. H., Liu, C. H., Wang, W., et al. (2009). Three-dimensional ionospheric electron density structure of the Weddell Sea Anomaly. *Journal of Geophysical Research*, *114*(A2), A02312. https://doi.org/10.1029/2008ja013455

Liu, H., Thampi, S. V., & Yamamoto, M. (2010). Phase reversal of the diurnal cycle in the midlatitude ionosphere. *Journal of Geophysical Research: Space Physics*, *115*(A1), A01305. https://doi.org/10.1029/2009ja014689

Ren, Z., Wan, W., Liu, L., Le, H., & He, M. (2012). Simulated midlatitude summer nighttime anomaly in realistic geomagnetic fields. *Journal of Geophysical Research*, *117*(A3), 41. https://doi.org/10.1029/2011ja017010

Richards, P. G., Meier, R. R., Chen, S., Drob, D. P., & Dandenault, P. (2017). Investigation of the causes of the longitudinal variation of the electron density in the Weddell Sea Anomaly. *Journal of Geophysical Research: Space Physics*, *122*(6), 6562–6583. https://doi.org/10.1002/2016ja023565

Richmond, A. D., Ridley, E. C., & Roble, R. G. (1992). A thermosphere/ionosphere general circulation model with coupled electrodynamics. *Geophysical Research Letters*, *19*(6), 601–604. https://doi.org/10.1029/92gl00401

Slominska, E., Blecki, J., Lebreton, J., Parrot, M., & Slominski, J. (2014). Seasonal trends of nighttime plasma density enhancements in the topside ionosphere. *Journal of Geophysical Research: Space Physics*, *119*(8), 6902–6912. https://doi.org/10.1002/2014ja020181

Slominska, E., Strumik, M., Slominski, J., Haagmans, R., & Floberghagen, R. (2020). Analysis of the impact of long-term changes in the geomagnetic Field on the spatial pattern of the Weddell Sea Anomaly. *Journal of Geophysical Research: Space Physics*, *125*(5), e2019JA027528. https://doi.org/10.1029/2019ja027528

Thampi, S. V., Balan, N., Lin, C., Liu, H., & Yamamoto, M. (2011). Mid-latitude summer nighttime anomaly (MSNA)—Observations and model simulations. *Annales Geophysicae*, *29*(1), 157–165. https://doi.org/10.5194/angeo-29-157-2011

Thampi, S. V., Lin, C., Liu, H., & Yamamoto, M. (2009). First tomographic observations of the midlatitude summer nighttime anomaly over Japan. *Journal of Geophysical Research*, *114*(A10), 89. https://doi.org/10.1029/2009ja014439

Xiong, C., & Lühr, H. (2014). The midlatitude summer night anomaly as observed by CHAMP and GRACE: Interpreted as tidal features. *Journal of Geophysical Research: Space Physics*, *119*(6), 4905–4915. https://doi.org/10.1002/2014ja019959

Yin, Y., González-Casado, G., Rovira-Garcia, A., Juan, J. M., Sanz, J., & Shao, Y. (2022). Summer nighttime anomalies of ionospheric electron content at midlatitudes: Comparing years of low and high solar activities using observations and tidal/planetary wave features. *Remote Sensing*, *14*(5), 1237. https://doi.org/10.3390/rs14051237

Zakharenkova, I., Cherniak, I., & Shagimuratov, I. (2017). Observations of the Weddell Sea Anomaly in the ground-based and space-borne TEC measurements. *Journal of Atmospheric and Solar-Terrestrial Physics*, *161*, 105–117. https://doi.org/10.1016/j.jastp.2017.06.014